Reliability and Agreement Between Metrics of Cone Spacing in Adaptive Optics Images of the Human Retinal Photoreceptor Mosaic

Daniela Giannini,[1] Giuseppe Lombardo,[2,3] Letizia Mariotti,[4] Nicholas Devaney,[4] Sebastiano Serrao,[1] and Marco Lombardo[1]

[1]Fondazione G.B. Bietti IRCCS, Rome, Italy
[2]Consiglio Nazionale delle Ricerche, Istituto per i Processi Chimico-Fisici, Messina, Italy
[3]Vision Engineering Italy srl, Rome, Italy
[4]Applied Optics Group, School of Physics, National University of Ireland, Galway, Ireland

Correspondence: Marco Lombardo, Fondazione G.B. Bietti IRCCS, Via Livenza 3, 00198 Rome, Italy; mlombardo@visioeng.it.

Submitted: October 7, 2016
Accepted: May 22, 2017

Citation: Giannini D, Lombardo G, Mariotti L, Devaney N, Serrao S, Lombardo M. Reliability and agreement between metrics of cone spacing in adaptive optics images of the human retinal photoreceptor mosaic. *Invest Ophthalmol Vis Sci*. 2017;58:3127–3137. DOI:10.1167/iovs.16-20890

Purpose. To assess reliability and agreement among three metrics used to evaluate the distribution of cell distances in adaptive optics (AO) images of the cone mosaic.

Methods. Using an AO flood illumination retinal camera, we acquired images of the cone mosaic in 20 healthy subjects and 12 patients with retinal diseases. The three spacing metrics studied were the center-to-center spacing (S_{cc}), the local cone spacing (LCS), and the density recovery profile distance (DRPD). Each metric was calculated in sampling areas of different sizes (64 × 64 μm and 204 × 204 μm) across the parafovea.

Results. Both S_{cc} and LCS were able to discriminate between healthy subjects and patients with retinal diseases; DRPD did not reliably detect any abnormality in the distribution of cell distances in patients with retinal diseases. The agreement between S_{cc} and LCS was high in healthy subjects (intraclass correlation coefficient [ICC] $\geq$ 0.79) and moderate in patients with retinal diseases (ICC $\leq$ 0.51). The DRPD had poor agreement with S_{cc} (ICC $\leq$ 0.47) and LCS (ICC $\leq$ 0.37). The correlation between the spacing metrics of the two sampling areas was greater in healthy subjects than in patients with retinal diseases.

Conclusions. The S_{cc} and LCS provided interchangeable estimates of cone distance in AO retinal images of healthy subjects but could not be used interchangeably when investigating retinal diseases with significant cell reflectivity loss (≥30%). The DRPD was unreliable for describing cell distance in a human retinal cone mosaic and did not correlate with S_{cc} and LCS. Caution is needed when comparing spacing metrics evaluated in sampling areas of different sizes.

Keywords: adaptive optics, cell spacing, cone metrics

Adaptive optics (AO) retinal imaging has enabled direct visualization of the cone mosaic and measurement of density, spacing, and packing arrangement of cones in normal eyes and eyes with retinal diseases.[1–3] Because an increasing number of studies is providing descriptive information about the integrity and pathologic change of the retinal cone mosaic using various approaches, it is of clinical importance to understand whether the results from different studies can be reliably compared.[4–8] In previous work,[9,10] we evaluated the agreement of density and packing arrangement of cones between sampling areas of different size and geometry. The results from normal eyes have shown that caution is needed when comparing cone density evaluated in sampling areas of different sizes (the average difference can reach 10% between 320 × 320 μm and 64 × 64 μm sampling windows)[9,10]; the packing arrangement of cones by Voronoi analysis has been shown to be minimally affected by window size. The primary advantages and drawbacks of these metrics have been previously discussed.[2,5,6,9,10] Cone density analysis creates strict demands on image quality because it requires that all cones within the region of interest be identified. For this reason, manual inspection of the cones in each image is highly recommended to minimize errors.[2,5,9,10] In addition, the moderate to high variability of cone density even in healthy adults may make this metric insensitive to small deviations from normal.[2,8] The limit of Voronoi analysis is related to the accuracy of the cone identification algorithm, the manual reselection of the unidentified or misidentified cones, and the "boundary effect," which is an apparent distortion of the Voronoi mosaic due to the exclusion of cones beyond the sampling window, the effect of which increases as the sampling window decreases.[9,10] It has been previously shown that the cone detection algorithm that segments the cone aperture, rather than only identifying the cone centroid position, is the most accurate approach for identifying the cones.[11,12]

Despite broad use of spacing metrics in clinical studies, there have been few evaluations of the reliability and agreement among various metrics.[13] Overall, cone-spacing analysis is less affected by image quality variations than cone density, because these methods do not require identification of

every cone within the region of interest.[2,4,5,7,14] For this reason, spacing metrics can be less prone to errors than cone density when tracking disease progression or response to treatment in eyes with retinal diseases, in which cones may be poorly imaged due to loss of wave-guiding property or missing cells.[4] However, there is no supporting evidence that cone-spacing metrics alone may provide a robust measurement for comparison among eyes (or even the same eye over time) in clinical studies.[2,4,13,14]

Most studies have used two main methodologies to estimate the spacing of cells in AO images of the cone mosaic: the density-count method and the distribution-of-distances methods. The center-to-center spacing (S_{cc}) has been one of the most widely adopted measures of cell spacing in studies of the retinal mosaic.[15–17] The S_{cc} is based on the density-count method, which is derived from the number of cones per unit area. The distribution-of-distances methods are assumption free and provide estimates of both central tendency and variation. These methods include the nearest neighbour distance (NND), the local cone spacing (LCS), and the nearest-neighbor cone spacing extracted from the Density Recovery Profile (DRP), which has been recently termed Density Recovery Profile Distance (DRPD).[13,18–20]

The scope of the present work was to assess the reliability and agreement of three spacing metrics, such as S_{cc}, LCS, and DRPD, for evaluating the distribution of cell distances in AO flood illumination images of the parafoveal cone mosaic. The metrics were calculated over two different sampling areas to evaluate the effect of window size on cone-spacing estimates. To evaluate the influence of cell reflectivity loss and cone-packing arrangement abnormalities on spacing metrics, the dataset included AO images acquired from healthy adult subjects and patients with a diagnosis of acquired or inherited retinal diseases.

Methods

All research procedures described in this work adhered to the tenets of the Declaration of Helsinki. The protocol was approved by the local ethical committee (Azienda Sanitaria Locale Roma A, Rome, Italy) and all subjects recruited gave written informed consent after a full explanation of the procedure. Inclusion criteria were an age >18 years, and no previous eye surgery, eye inflammation, glaucoma, or cataract; in addition, control subjects were required to have no history or presence of systemic diseases. Subjects recruited for the study received a complete eye examination, including non-contact ocular biometry using the IOL Master (Carl Zeiss Meditec, Inc., Jena, Germany).

Human Subjects

Twenty healthy volunteers (age 33 ± 9 years; range 23–54 years; sex: 15 female and 5 male), and 12 patients with retinal diseases (age 41 ± 10 years; range 23–59 years; sex: 10 female and 2 male) were recruited in this study (Supplementary Table S1). The latter participants included subjects with a diagnosis of diffuse cuticular drusen and a family history of AMD (drusen; $n = 2$),[21,22] nonproliferative diabetic retinopathy (NPDR; $n = 4$) according to severity on the Early Treatment Diabetic Retinopathy Scale,[23,24] retinitis pigmentosa (RP; $n = 4$; USH2A gene mutation), Best macular dystrophy (Best; $n = 1$; BEST 1 gene mutation), and occult macular dystrophy (OMD; $n = 1$; RP1L1 gene mutation).[25] These participants were enrolled in this study to have a dataset of AO images of the cone mosaic with increasing amount of cell loss and variable abnormalities in the packing arrangement of the cones.

Image Acquisition and Processing

A flood-illuminated AO retinal camera (*rtx1*; Imagine Eyes, Paris, France) was used to collect images of the cone mosaic on 20 healthy subjects and 12 subjects with various retinal diseases. The imaging session was conducted after dilating the pupil with one drop of 1% tropicamide. During imaging, fixation was maintained by instructing the patient to fixate on the internal target of the instrument moved by the investigator. At each retinal location, a sequence of 40 frames (rate: 9.5 frames per second) was acquired by illuminating a retinal area subtending 4 degrees of visual angle in the right eye of each subject; images were acquired at several locations in the central retina covering an area of 5×4 degrees centered on the preferred locus of fixation (PRL; coordinates $x = 0°$ and $y = 0°$ and here used as the foveal reference point).

A proprietary program from the manufacturer has been used to correct for distortions within frames of the raw image sequence and to register and frame-average to produce a final image with enhanced signal-to-noise ratio before further analysis. In this study, two sampling areas of different size (64×64 μm and 204×204 μm) were cropped from each final image at 1.5 degrees superior and 2.5 degrees temporal from the PRL. The two eccentricities were chosen to be a compromise between the resolution limit of the instrument, which does not allow all the cones to be resolved too close to the fovea, and the presence of rods, which alter the cone relative spacing enough to be detectable by the instrument when further than 4 degrees from the fovea.

The nonlinear formula of Drasdo and Fowler[26] and the Gullstrand schematic model eye parameterized by the biometry measurements (corneal central curvature, anterior chamber central depth, axial length) were used to convert each final image from degrees of visual angle to micrometers on the retina.[27] The corrected magnification factor (RMF_{corr}) was calculated for each eye to correct for the differences in optical magnification and thus retinal image size between eyes, as previously described.[9,10,24–27]

Image cone labeling was automatically performed using an enhanced version of the algorithm implemented with the image processing toolbox in Matlab (The Mathworks, Inc, Natick, MA, USA).[9,10,23,24,28] Cones were identified independently in each sampling window. The cone identification algorithm's performance was verified by three expert investigators (DG, LM, ML), who reviewed each sampling area and manually identified cones that they agreed to be missed or selected in error by the algorithm. This procedure ensured that the number of excluded cones was minimized. A buffer zone was created in each sampling window to minimize the boundary effect for packing geometry metrics.[9,10] The x,y coordinates of the cones in each sampling window were then stored in a text array and used to calculate the cone metrics.

Density and Packing Arrangement Metrics of the Cone Mosaic

Cone counts were converted into local densities by calculating their number per square millimeter (cones per mm^2). The cone packing arrangement was analyzed using Voronoi diagrams.[9,10,29,30] The Voronoi tessellation was implemented by the voronoi Matlab function from the bidimensional coordinates of labeled cones, as previously described.[9,10,24,29] The Voronoi regions lying at the bounds of each section were excluded from further analysis, creating a buffer zone = 2 NND to minimize the boundary effect. The number of Voronoi tiles with six sides ($6n$) was divided by the total number of bound Voronoi tiles within each sampling area and expressed as a percentage.

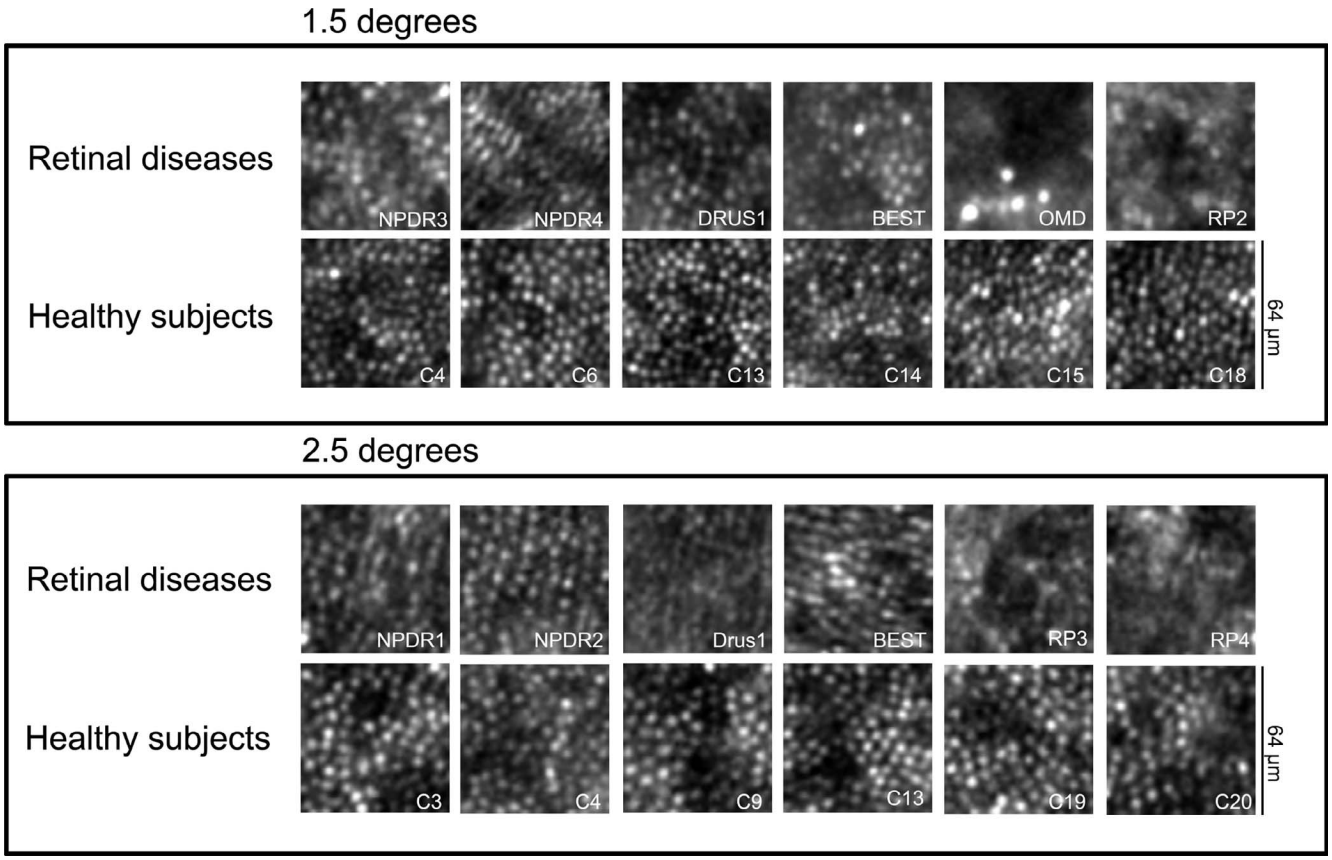

FIGURE 1. Adaptive optics images of the parafoveal cone mosaic in patients with retinal diseases and healthy subjects acquired at 1.5 degrees superior and 2.5 degrees temporal from the fovea. The photoreceptor mosaic in patients with retinal diseases showed variable cell loss and abnormalities in the packing arrangement of the cones with respect to healthy subjects. The sampling area subtends 64 × 64 μm. Data from participants are summarized in Supplementary Table S1.

Spacing Metrics of the Cone Mosaic

Three metrics were used to describe the distribution of cone distances:

1. The S_{cc} was determined from cone density using the following expression:

$$S_{cc} = 1000\left[\frac{2}{\sqrt{3}D}\right]^{1/2},$$

where D is the number of cones per square millimeter. Because the method assumes an exact relationship between cone density and spacing, the cones are expected to be arranged in triangular lattice (this metric was also termed minimum S_{cc}).[15–17,29] It is equivalent to the metric *S* used by Chui et al.[15] and *S(x,y)* used by Li et al.[16] Care should be taken to avoid regions of missing data (e.g., large blood vessels, image boundary) or defects in the image to avoid overestimating the spacing distribution of cones.
2. The LCS was determined by calculating the average of the minimum distances from the center of a given cone to the centers of six neighboring cones within an area of 12 pixels (9.6 μm) diameter (i.e., almost twice the size of the cone at both retinal locations).[24] The LCS has been developed to minimize the known limits of NND in estimating the mosaic spacing. Indeed, the NND takes into account only the nearest of each cell's known neighbors, regardless of its distance; therefore, it can be strongly influenced by very large NNDs of isolated cells, which decrease its sensitivity to represent the distribution of cell distances in retinal diseases.[13]
3. The DRPD was derived from the DRP reconstructed from the autocorrelogram.[18] The spatial autocorrelogram was generated by superimposing the distribution of all cells in a sampling area using each cell in the area in turn as the reference cell. To determine the nearest-neighbor cone distance, the DRPD was calculated as the first local maximum of the DRP created from the autocorrelogram with maximum radius = one-fifth of the image dimension and a series of annuli of 1-μm width. The width of each bin was determined from equation 16 in Rodieck,[18] under assumption of having a reliability factor value of 5 and 4 for healthy subjects and patients with retinal diseases, respectively. The bin's width was accordingly 1 μm in the two populations. The DRPD takes into account all of a cell's neighbors up to a limited distance that depends on the shape of the DRP, which is a graphical representation of spatial behavior derived from the spatial autocorrelogram.[18] It is equivalent to the nearest-neighbour cone spacing determined from the DRP in previous studies.[4,14] Nevertheless, the DRP provides a different measure than the NND and a more complete overview of the spatial arrangement of the cone mosaic; its estimates are based on all of the other points about a given point, rather than just one.

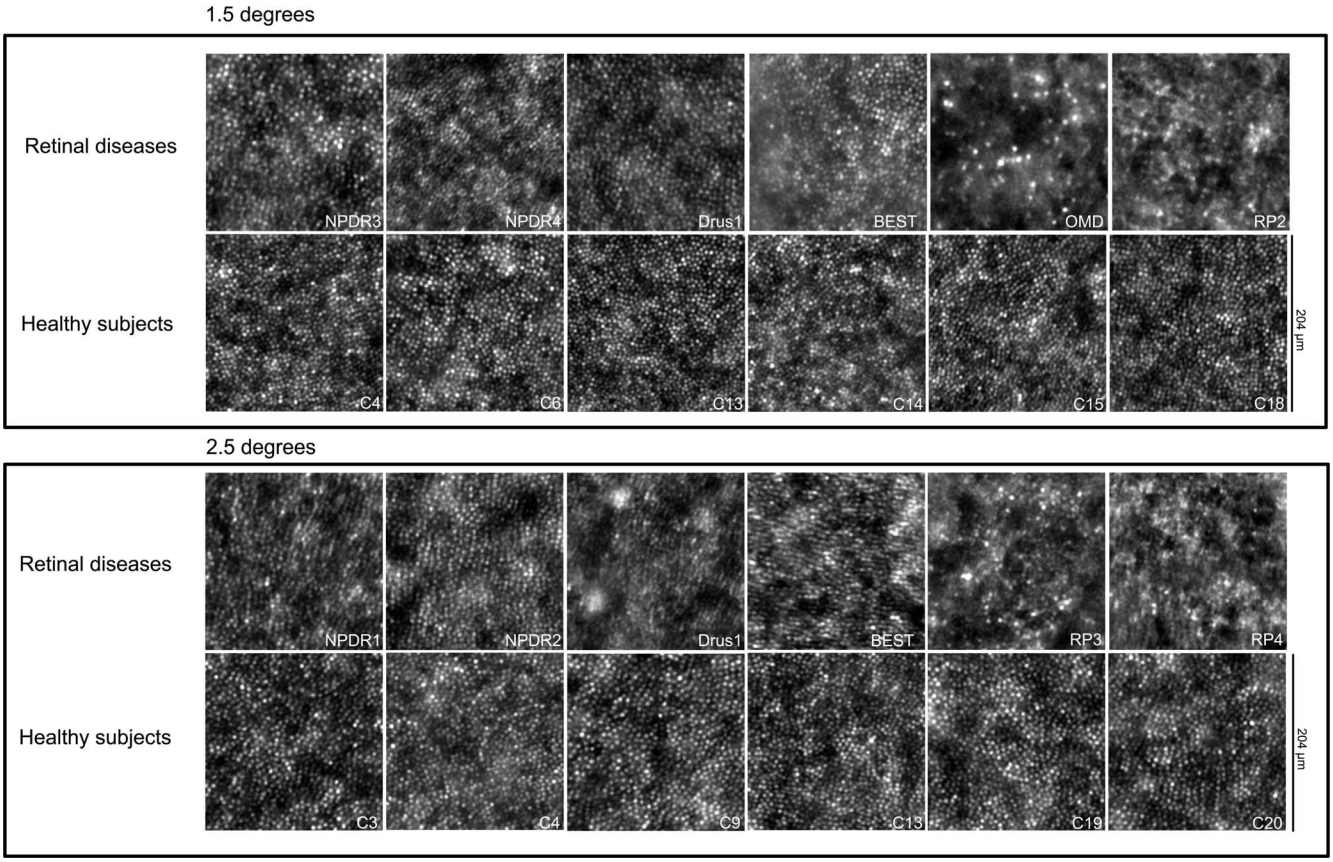

FIGURE 2. Adaptive optics images of the parafoveal cone mosaic in patients with retinal diseases and healthy subjects acquired at 1.5 degrees superior and 2.5 degrees temporal from the fovea. The sampling area subtends 204 × 204 µm. Data from participants are summarized in Supplementary Table S1.

Statistics

Data were expressed as mean ± SD. Statistics were performed using the SPSS software (version 17.1; SPSS, Inc., Chicago, IL, USA) and Matlab (version R2013a; The Mathworks, Inc., Natick, MA, USA).

The sample size was calculated to detect a mean difference in cone density of 2500 cones/mm^2 (SD = 2500 cones/mm^2) between healthy subjects and patients with retinal diseases (2:1 allocation) with a two-sided significance level of 5% and a power of 82%.

The intraclass correlation coefficient (ICC; two-way, random-effects model) was calculated to estimate the absolute agreement between each pair of spacing metrics in the two sampling areas for each study group. The correlation and Bland-Altman analysis were used to assess the 95% limits of agreement (LoA) between the pair of spacing metrics that have shown high absolute agreement (ICC > 0.7), and between the values of each spacing metric extracted from the two sampling areas.

The differences between the spacing metrics of the two study groups was evaluated using the nonparametric Mann-Whitney *U* test.

RESULTS

Cone Density and Packing Arrangement

Over a 64 × 64-µm sampling area, the cone densities at 1.5 degrees and 2.5 degrees retinal eccentricities in healthy subjects were 32281 ± 2281 cones/mm^2 and 29411 ± 2147 cones/mm^2, respectively (Fig. 1). Cone density in patients with retinal diseases was on average 26% ± 3% (range from 2% to 65%; $P < 0.001$) lower than in healthy subjects.

Over a 204 × 204-µm sampling area, the cone densities at 1.5 degrees and 2.5 degrees from the PRL in healthy subjects were 31,494 ± 2489 cones/mm^2 and 28,703 ± 1822 cones/mm^2, respectively (Fig. 2). Cone density in patients with retinal diseases was on average 16% ± 5% (range from 1% to 58%; $P < 0.001$) lower than that in healthy subjects.

The average percentage of six-sided Voronoi tiles was almost constant across different sampling areas in either study groups. In healthy subjects, the 6*n* Voronoi average ranged from 50% to 45% for 1.5 degrees and 2.5 degrees, respectively. In patients with retinal diseases, the average 6*n* Voronoi tiles were significantly lower than control values ($P < 0.05$), except for values calculated in 204 × 204-µm sampling areas at 2.5 degrees retinal eccentricity ($P = 0.14$). Cone density and percent of six-sided Voronois for all cases are shown in Table 1.

Cone Spacing Metrics

In healthy subjects, the values of all spacing metrics increased with increasing eccentricity and showed high consistency between the two different sampling areas; S_{cc} ranged from 5.99 ± 0.21 µm to 6.35 ± 0.24 µm from 1.5 degrees to 2.5 degrees from the fovea, respectively; LCS ranged from 6.12 ± 0.18 µm to 6.41 ± 0.18 µm, respectively; and DRPD ranged from 5.80 ± 0.80 µm to 6.20 ± 0.66 µm, respectively. In patients with retinal diseases, the spacing metrics showed higher variation

Table 1. Mean (±SD) Cone Density and Percentage of Six-Sided (*6n*) Voronois in Study Participants Over Different Sampling Areas at Two Retinal Locations

Sampling Area	64 × 64 μm				204 × 204 μm			
Metric	Cone Density, Cones/mm²		*6n* Voronois, %		Cone Density, Cones/mm²		*6n* Voronois, %	
Retinal Eccentricity	1.5 Degrees	2.5 Degrees	1.5 Degrees	2.5 Degrees	1.5 Degrees	2.5 Degrees	1.5 Degrees	2.5 Degrees
Healthy subjects								
C_1	30,476	26,905	51.1	47.3	29,924	27,438	48.7	43.2
C_2	36,341	30,732	57.0	46.5	35,517	30,154	57.1	48.1
C_3	29,286	26,429	48.2	45.3	27,683	26,591	51.5	45.9
C_4	31,951	28,780	55.9	45.6	31,707	28,331	55.7	48.0
C_5	34,146	33,659	47.0	40.8	33,397	32,153	47.0	42.4
C_6	28,537	30,976	59.3	45.6	27,632	29,587	53.0	41.7
C_7	31,951	29,024	43.0	40.9	30,431	27,392	39.1	45.5
C_8	32,927	28,780	41.8	51.2	34,880	27,861	47.3	48.4
C_9	31,220	28,537	48.9	32.5	29,021	27,375	48.2	39.7
C_10	36,098	30,732	50.9	43.0	34,641	29,139	48.7	48.0
C_11	34,146	28,537	44.5	40.7	31,599	27,446	43.8	40.0
C_12	32,195	26,585	41.8	44.8	31,367	29,305	44.1	41.6
C_13	34,878	29,512	57.6	50.0	33,861	27,387	54.5	53.9
C_14	35,366	27,561	58.2	50.6	34,053	26,595	52.5	52.7
C_15	32,927	27,805	60.4	44.9	34,378	27,081	53.2	47.2
C_16	30,488	30,488	44.8	46.0	30,571	30,476	42.2	46.1
C_17	30,000	29,756	39.3	39.3	28,490	28,727	51.1	44.4
C_18	30,000	34,390	59.5	53.0	29,333	32,952	51.6	46.1
C_19	30,732	27,805	40.5	48.7	29,986	27,374	38.0	45.3
C_20	31,951	31,220	54.4	39.1	31,411	30,694	51.1	40.9
Mean ± SD	32,281 ± 2,281	29,411 ± 2,147	50.3 ± 7.0	44.8 ± 4.9	31,494 ± 2,489	28,703 ± 1,822	48.9 ± 5.3	45.5 ± 3.9
Retinal diseases								
Drusen_1	24,146	27,317	48.5	44.2	22,679	28,900	50.1	43.4
Drusen_2	24,390	28,780	41.2	49.4	27,524	28,762	42.9	41.5
NPDR_1	26,341	23,902	39.2	34.4	26,571	24,000	47.5	47.9
NPDR_2	26,098	23,171	44.4	47.6	26,738	23,452	42.9	46.6
NPDR_4	31,707	24,146	34.8	47.7	32,110	25,396	47.9	46.4
NPDR_5	24,146	25,122	48.4	36.6	24,442	23,444	43.2	43.5
Best	23,500	25,750	58.1	34.8	25,444	24,412	45.6	48.8
OMD	11,463	10,244	44.0	31.8	13,134	16,914	35.5	33.4
RP_1	19,024	17,073	43.7	30.2	26,754	27,112	41.2	39.1
RP_2	24,146	23,902	47.6	35.9	25,273	27,411	39.1	41.7
RP_3	25,366	21,951	41.4	37.9	26,850	25,298	41.0	39.3
RP_4	19,512	18,293	32.6	34.7	25,273	26,247	41.7	41.3
Mean ± SD	23,320 ± 4,937	22,471 ± 5,089	43.7 ± 6.8	38.8 ± 6.7	25,233 ± 4,422	25,112 ± 3,203	43.2 ± 4.1	42.7 ± 4.4
P	<0.001	<0.001	0.02	0.01	<0.001	<0.001	0.003	0.14

around the mean values, which was caused by the abnormal and variable distribution of distances between cells across the parafoveal retinal locations in the disease population (Table 2).

The differences of S_{cc} and LCS values between healthy subjects and patients with retinal diseases were statistically significant ($P \leq 0.01$) in both sampling areas at both retinal eccentricities, except for the LCS values measured in the 204 × 204-μm-area at 2.5 degrees retinal eccentricity ($P = 0.27$). This result was consistent with the distribution of *6n* Voronois between healthy and pathologic cases in the same area (see Table 1). The differences of DRPD values between healthy subjects and patients with retinal diseases were not statistically significant in any case.

Agreement and Correlation Between Spacing Metrics. The S_{cc} and LCS values showed high agreement with each other in healthy subjects over both sampling areas and both retinal eccentricities (averaged ICC = 0.86; ICC range = 0.80–0.93). On the other hand, the agreement between S_{cc} and LCS values in patients with retinal diseases was poor (averaged ICC = 0.28; ICC range = 0.08–0.51). The agreement between the DRPD and the other two spacing metrics was low in both study groups (averaged ICC = 0.27; ICC range = 0.05–0.47). The ICC analysis between each pair of spacing metrics is summarized in Table 3.

In healthy subjects, the correlation between S_{cc} and LCS was high over both sampling areas ($R^2 = 0.75$, $P < 0.001$; and $R^2 = 0.88$, $P < 0.001$, over 64 × 64 μm and 204 × 24 μm, respectively) (Figure 3). In patients with retinal diseases, the correlation between S_{cc} and LCS was poor over both sampling areas ($R^2 = 0.018$, $P = 0.53$; and $R^2 = 0.25$, $P = 0.014$, respectively).

The 95% LoA was slightly influenced by window size; the agreement between S_{cc} and LCS values over 204 × 204-μm areas was greater than 64 × 64 μm areas (Fig. 3). This was associated with the greater percentage of *6n* Voronois in patients with retinal diseases over a 204 × 204-μm sampling window.

Influence of the Sampling Area on S_{cc}. The S_{cc} values calculated over sampling areas of different sizes showed high correlation both in healthy subjects ($R^2 = 0.84$, $P < 0.001$) and

Table 2. Mean (±SD) Values of the Three Spacing Metrics in Different Sampling Areas at Two Retinal Locations

Sampling Area	64 × 64 µm						204 × 204 µm					
Metric	S_{cc}, µm		LCS, µm		DRPD, µm		S_{cc}, µm		LCS, µm		DRPD, µm	
Retinal Eccentricity	1.5 deg	2.5 deg	1.5 deg	2.5 deg	1.5 deg	2.5 deg	1.5 deg	2.5 deg	1.5 deg	2.5 deg	1.5 deg	2.5 deg
Healthy subjects												
C_1	6.16	6.55	6.22	6.57	5.50	6.50	6.21	6.49	6.29	6.46	5.50	6.50
C_2	5.64	6.13	5.86	6.31	5.50	6.50	5.70	6.19	5.82	6.25	5.50	5.50
C_3	6.28	6.61	6.39	6.65	6.50	6.50	6.46	6.59	6.51	6.59	5.50	6.50
C_4	6.01	6.33	6.07	6.43	5.50	5.50	6.03	6.38	6.12	6.45	5.50	6.50
C_5	5.82	5.86	5.90	6.05	5.50	5.50	5.88	5.99	5.96	6.08	5.50	5.50
C_6	6.36	6.11	6.09	6.38	5.50	5.50	6.46	6.25	6.26	6.53	5.50	5.50
C_7	6.01	6.31	6.41	6.28	6.50	6.50	6.16	6.49	6.50	6.31	6.50	6.50
C_8	5.92	6.33	6.01	6.38	5.50	6.50	5.75	6.44	5.86	6.50	5.50	6.50
C_9	6.08	6.36	6.18	6.52	6.50	5.50	6.31	6.49	6.36	6.52	6.50	6.50
C_10	5.66	6.13	5.89	6.40	4.50	5.50	5.77	6.30	5.86	6.42	5.50	5.50
C_11	5.82	6.36	6.07	6.95	5.50	6.50	6.05	6.49	6.15	6.51	6.50	6.50
C_12	5.99	6.59	6.08	6.63	5.50	6.50	6.07	6.28	6.17	6.36	5.50	6.50
C_13	5.75	6.26	5.92	6.43	5.50	5.50	5.84	6.49	5.96	6.60	5.50	5.50
C_14	5.71	6.47	5.89	6.61	5.50	5.50	5.82	6.59	5.91	6.65	5.50	5.50
C_15	5.92	6.44	6.07	6.38	5.50	7.50	5.80	6.53	5.90	6.55	5.50	6.50
C_16	6.15	6.15	6.33	6.27	6.50	5.50	6.15	6.16	6.20	6.24	6.50	5.50
C_17	6.20	6.23	6.37	6.46	5.50	7.50	6.37	6.34	6.42	6.37	5.50	6.50
C_18	6.20	5.79	6.28	5.91	5.50	6.50	6.27	5.92	6.34	5.99	5.50	5.50
C_19	6.13	6.44	6.31	6.53	8.50	6.50	6.21	6.49	6.25	6.52	8.50	6.50
C_20	6.01	6.08	6.11	6.27	5.50	6.50	6.06	6.13	6.14	6.24	5.50	6.50
Mean ± SD	5.99 ± 0.21	6.28 ± 0.22	6.12 ± 0.18	6.42 ± 0.22	5.80 ± 0.8	6.20 ± 0.66	6.07 ± 0.24	6.35 ± 0.19	6.15 ± 0.22	6.41 ± 0.18	5.85 ± 0.75	6.10 ± 0.5
Retinal diseases												
Drusen_1	6.92	6.50	6.91	6.57	5.50	5.50	7.14	6.32	7.01	6.32	6.50	5.50
Drusen_2	6.88	6.33	6.64	6.31	5.50	4.50	6.48	6.34	6.33	6.29	5.50	5.50
NPDR_1	6.62	6.95	6.55	6.82	6.50	6.50	6.59	6.94	6.59	6.83	5.50	6.50
NPDR_2	6.65	7.06	6.56	6.88	6.50	5.50	6.57	7.02	6.54	6.86	6.50	6.50
NPDR_4	6.03	6.92	6.08	6.81	5.50	6.50	6.00	6.74	6.02	6.73	5.50	6.50
NPDR_5	6.92	6.78	6.74	6.59	6.50	6.50	6.87	7.02	6.65	6.79	6.50	6.50
Best	7.01	6.70	6.94	6.61	6.50	6.50	6.74	6.88	6.67	6.70	6.50	6.50
OMD	10.04	10.62	6.91	6.48	6.50	4.50	9.38	8.26	6.59	6.38	6.50	4.50
RP_1	7.79	8.22	6.62	6.56	4.50	4.50	6.57	6.53	6.26	6.14	5.50	4.50
RP_2	6.92	6.95	6.69	6.34	6.50	4.50	6.76	6.49	6.47	6.34	5.50	5.50
RP_3	6.75	7.25	6.50	6.70	5.50	7.50	6.56	6.76	6.36	6.46	6.50	5.50
RP_4	7.69	7.95	6.60	6.61	5.50	4.50	6.76	6.63	6.44	6.46	5.50	5.50
Mean ± SD	7.19 ± 1.01	7.35 ± 1.16	6.65 ± 0.23	6.61 ± 0.18	5.92 ± 0.67	5.58 ± 1.08	6.87 ± 0.84	6.83 ± 0.51	6.49 ± 0.25	6.53 ± 0.24	6.00 ± 0.52	5.75 ± 0.75
P	<0.001	<0.001	<0.001	0.01	0.32	0.09	<0.001	<0.001	<0.001	0.27	0.25	0.25

Table 3. ICC Showing, for Each Study Group, the Absolute Agreement Between Cone Spacing Metrics in Two Different Sampling Areas at Two Retinal Locations

Sampling Area	64 × 64 μm		204 × 204 μm	
Retinal Eccentricity	1.5 Degrees	2.5 Degrees	1.5 Degrees	2.5 Degrees
Healthy subjects				
ICC between S_{cc} and LCS	0.80	0.80	0.93	0.93
ICC between S_{cc} and DRPD	0.33	0.26	0.24	0.44
ICC between LCS and DRPD	0.37	0.11	0.25	0.25
Retinal diseases				
ICC between S_{cc} and LCS	0.08	0.23	0.51	0.29
ICC between S_{cc} and DRPD	0.05	0.47	0.36	0.14
ICC between LCS and DRPD	0.27	0.26	0.36	0.25

patients with retinal diseases ($R^2 = 0.66$, $P < 0.001$). On the other hand, the distribution of data points in the Bland-Altman plot showed that agreement was poor for S_{cc} values estimated from cone mosaics with more than 30% cone reflectivity loss (Fig. 4).

Influence of the Sampling Area on LCS. The correlation between LCS values of the two sampling areas was high in healthy subjects ($R^2 = 0.76$, $P < 0.001$) and moderate in patients with retinal diseases ($R^2 = 0.46$, $P < 0.001$) at both retinal eccentricities (Fig. 5). The 95% LoA showed scattered values around the bias line that tended to increase as the average LCS value increased.

Influence of the Sampling Area on DRPD. The correlation of DRPD values between the two sampling areas was moderate in healthy subjects ($R^2 = 0.59$, $y = 0.659x + 2.02$, $P < 0.001$) and low in patients with retinal diseases ($R^2 = 0.34$, $y = 0.419x + 3.466$, $P = 0.003$) at both retinal eccentricities. Both the scatter plot and the Bland-Altman plot (not shown) did not evidence any difference in the distribution of data points between healthy subjects and patients with retinal diseases.

Discussion

We evaluated the agreement among three metrics currently used to describe the distribution of distances between cones in AO images of the cone mosaic. A group of healthy subjects and a group of patients with different retinal diseases and variable loss of cone reflectivity (from 2% to 65% with respect to healthy photoreceptor mosaic) were included in the study to understand if S_{cc}, LCS, and DRPD, which have been calculated over sampling areas of different size, could be used interchangeably in clinical studies.

Both S_{cc} and LCS were able to discriminate between healthy subjects and patients with retinal diseases; on the other hand, DRPD did not reliably detect any abnormality in the distribution of distances in the study population. This is related to the fact that this metric is calculated from the shape of the DRP, which remains unchanged even for large undersampling (only the vertical scale, i.e., cone density, is influenced by cell loss).[18] Previously, Cooper et al.[13] showed, in simulated Adaptive Optics Scanning Laser Ophthalmoscopy (AOSLO) images of the cone mosaic, that the DRPD was remarkably insensitive to undersampling of cone coordinates, being unable to classify as pathologic mosaics with up to 60% loss of cone reflectivity. In the same study,[13] the authors found that NND was also insensitive to undersampling (up to 50%). Therefore, the use of single spatial metrics based on DRPD or NND would not be clinically valuable to accurately discriminate between healthy and pathologic photoreceptor mosaics. To overcome this major limit of NND in evaluating the distribution of cell distances in a human retinal cone mosaic, we previously developed the LCS metric.[24] In this study, the S_{cc} and LCS were highly correlated and could be used interchangeably without incurring any methodological error until 20% to 25% of the cones in the given mosaic have been lost (e.g., cases with hard drusen and NPDR in this study). However, both correlation and agreement between this pair of spacing metrics dropped when cell reflectivity loss was ≥30%, primarily when comparison was made in 64 × 64-μm sampling areas (e.g., cases with inherited retinal dystrophies). In this study, cases with retinal diseases had significantly fewer six-sided Voronois than healthy cone mosaics, as expected, because lattice quality diminishes with disease progression (as well as with retinal eccentricity even in healthy subjects).[13,17,24] The S_{cc}, which provides a single-point estimate without a measure of variation and assumes an ordered lattice, is more prone to overestimating the integrity of the cone mosaic in retinal diseases than LCS. On the other hand, LCS alone may lose the sensitivity to detect small deviations from normal (<20% undersampling, as for example in hard drusen and NPDR cases in this study). Because the methodology of calculating LCS also indirectly provides estimates of both the SD and mean of the distances between cells, the use of their ratio, previously termed Linear Dispersion index,[24] has been shown to achieve enough sensitivity to evaluate the averaged distribution of cell distances across the parafovea in controlled clinical study.

The influence of the sampling window size was relevant for the analysis of intercell distance in AO images of the cone mosaic, possibly because photoreceptor loss is variable across areas of the retinal mosaic as well as among retinal diseases. Overall, the choice of the window size should avoid poor sampling. The use of smaller sampling windows, such as the conventional 64 × 64-μm area, allows for a local analysis of the integrity of the cone mosaic, whereas the use of larger areas, such as 204 × 204 μm, may lead to overestimating the integrity of the retinal mosaic, probably because of the presence of healthy domains of the cone mosaic in the area of analysis. As shown in Figures 4 and 5, the use of smaller sampling areas would be preferable for tracking disease progression when using S_{cc} and LCS (and possibly NND). If data analysis were carried out over large sampling areas, the complementary use of more than one metric to describe the spatial arrangement of the cones would be preferable. We have already shown that the pathologic decrease of cone density in adult subjects, even when density falls within normal limits, induces abnormal changes in the arrangement of the cones;[24] therefore, the

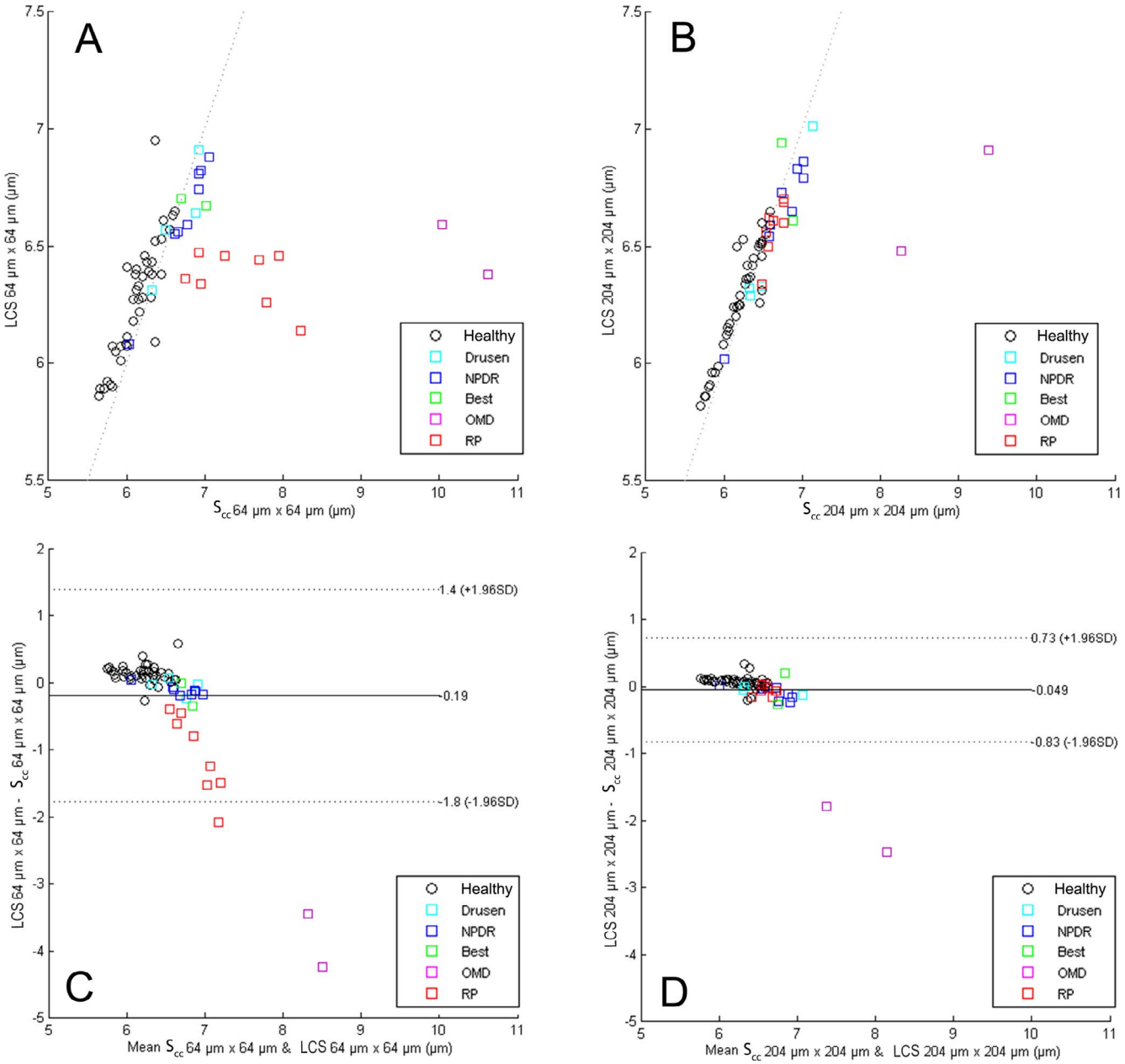

Figure 3. **(A)** Correlation between LCS and S_{cc} in 64×64 µm sampling areas. Data were aggregated from 1.5 degrees and 2.5 degrees retinal eccentricities. In healthy subjects, the correlation between LCS and S_{cc} was high ($R^2 = 0.75$, $y = 0.846x + 1.082$, $P < 0.001$); almost all values (85%) were on the bisector ($y = x$, $R^2 = 1$). In patients with retinal diseases, the correlation between LCS and S_{cc} was very low ($R^2 = 0.018$, $y = -0.028x + 6.733$, $P = 0.53$); the patients with advanced stages of inherited retinal dystrophies (OMD and RP) and diffuse loss of cone reflectivity (≥30%) primarily contributed to the decreased correlation between this pair of spacing metrics. **(B)** Correlation between LCS and S_{cc} in 204×204 µm sampling areas. In healthy subjects, the correlation was high ($R^2 = 0.89$, $y = 0.859x + 0.946$, $P < 0.001$); 95% of the LCS and S_{cc} values were on the bisector. In patients with retinal diseases, correlation between LCS and S_{cc} was low ($R^2 = 0.25$, $y = 0.171x + 5.433$, $P = 0.01$). **(C, D)** Bland-Altman plots of S_{cc} and LCS values calculated over 64×64 µm and 204×204 µm sampling areas respectively. Although the agreement between this pair of spacing metrics was high in the 64×64 µm area, the use of greater sampling areas further increased agreement between metrics. The symbols are described in the plot.

complementary use of regularity indices based on Voronoi analysis, together with spacing and density metrics is very helpful to detect small deviations from normal cone mosaic arrangement.[24,31]

The spacing metrics examined in this work do not represent the full list of metrics for evaluating the distribution of cell distances of a retinal mosaic. Several other metrics have been generated from the point coordinates of cells or directly from the AO image of the cone mosaic, such as those based on analysis of the Fourier spectrum of the image.[13,32–39] Currently, the main limit of any metric describing the spatial position of the cones is related to the correct cell identification. As disease progresses, cell loss and disorder in cell spacing increases, which in turn decreases resolution by distorting the AO image of the cone mosaic. Accurate cone identification and segmentation is required to minimize methodological errors.[2,9,10,12,13] The present AO images were acquired at 1.5 degrees superior and 2.5 degrees temporal from the PRL and the results from the

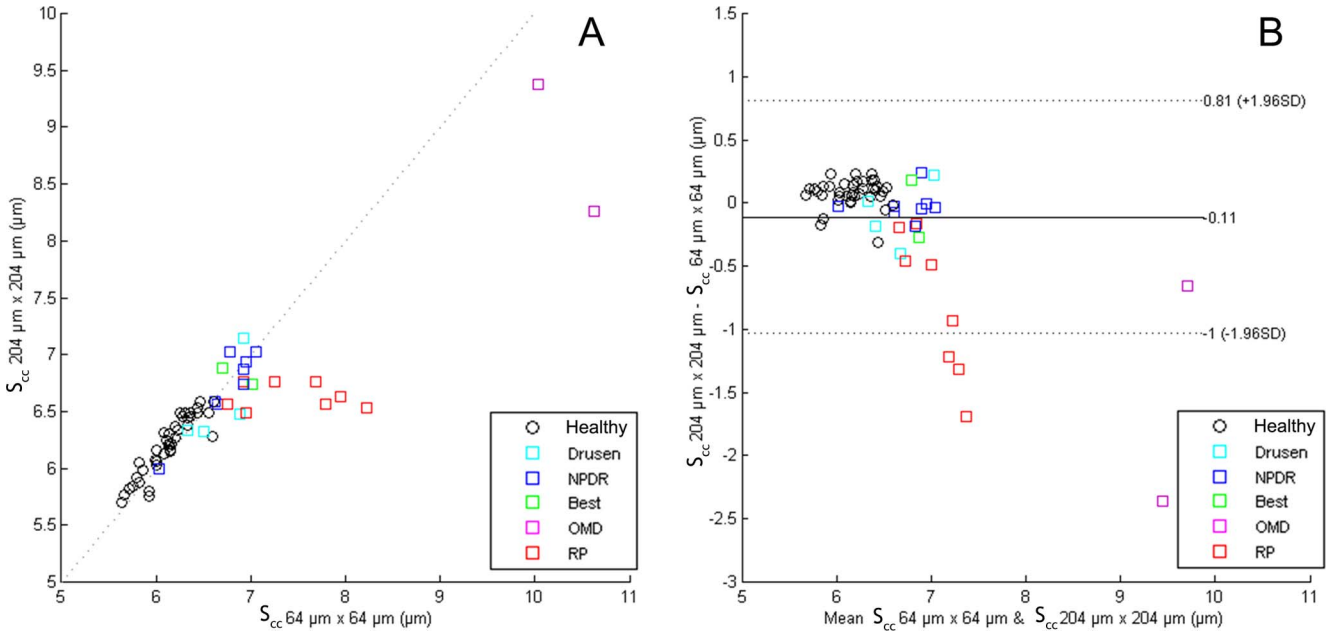

Figure 4. **(A)** Correlation between S_{cc} values calculated in the two sampling areas of 64 × 64 µm and 204 × 204 µm. In healthy subjects, the correlation was high ($R^2 = 0.84$, $y = 0.924x + 0.541$, $P < 0.001$), with 85% of S_{cc} values that were on the bisector. In patients with retinal diseases, the correlation was moderate ($R^2 = 0.67$, $y = 0.517x + 3.088$, $P < 0.001$); the patients with advanced stages of inherited retinal dystrophies (OMD and RP) and diffuse loss of cone reflectivity (≥30%) contributed to decrease the overall correlation between S_{cc} values taken over sampling areas of different sizes. **(B)** Bland-Altman plot of S_{cc} values. The outliers in the Bland-Altman plot are represented by three patients (OMD, RP1, and RP4; see Supplementary Table S1) who had the lowest cone density in the study population. Data were aggregated from 1.5 degrees and 2.5 degrees from the fovea. The symbols are described in the plot.

present work cannot be directly extended to different areas of the retina. In previous studies,[10,16,40] the PRL was found to deviate, on average, 27 ± 15 µm from the foveal center, and the displacement of the PRL to foveal center was not correlated with SEr or AxL. Coregistration of AO images with OCT cross-section images would be desirable in clinical studies to avoid variation in determination of eccentricity caused by compromised vision that may have the PRL away from the anatomic foveal center. It was also outside the scope of this work to determine the best spacing metric to be used in clinical

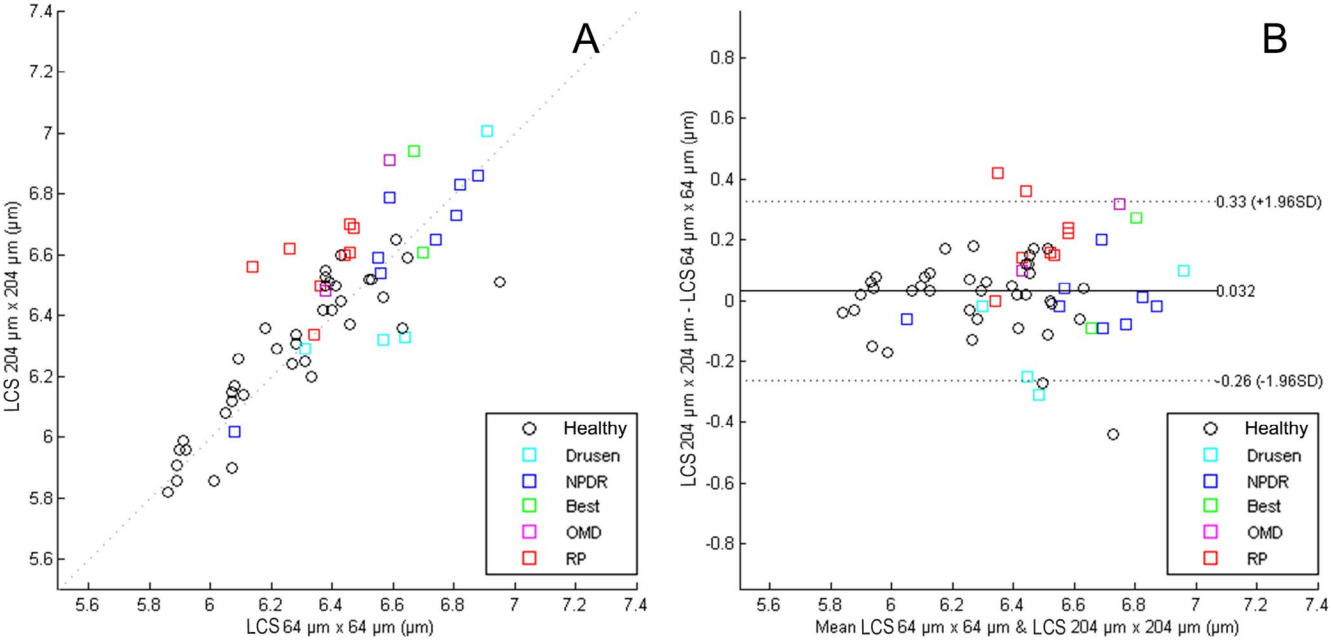

Figure 5. **(A)** Correlation of the LCS values calculated in the two sampling areas. In healthy subjects, the correlation between the LCS values was good ($R^2 = 0.76$, $y = 0.823x + 1.116$, $P < 0.001$); on the other hand, it was moderate ($R^2 = 0.46$, $y = 0.715x + 1.935$, $P < 0.001$) in patients with retinal diseases. **(B)** Bland-Altman plot of the LCS values. Agreement between the LCS values calculated over sampling areas of different sizes was primarily decreased by patients with retinal diseases (i.e., for increasing values of LCS). Data were aggregated from 1.5 degrees and 2.5 degrees from the fovea. The symbols are described in the plot.

studies. Overall, as cone density and packing arrangement of the cones deviate from normal expected values, S_{cc} is less reliable than LCS to determine the distribution of cell distances in the human photoreceptor mosaic. The complementary use of density, spacing, and regularity metrics is valuable to increase the sensitivity of each descriptor for evaluating small deviations of the cone mosaic from the normal expected packing density arrangement.[13,24,25,29,31]

The use of other AO imaging modalities, such as nonconfocal split-detector based AOSLO, would enhance the identification of cell loss over other confocal or nonconfocal techniques.[2,41] For this reason, we preferred using the term loss of cone reflectivity instead of cone loss. Comparing the results of cone metrics calculated on images of the same mosaic collected by different AO imaging modalities would be valuable to understand differences between instruments.

In conclusion, the sampling window size and the method used for evaluating the distribution of cell distances in AO images of the human retinal cone mosaic should be considered when comparing spacing metrics between clinical studies.

Acknowledgments

The authors thank Lucia Ziccardi for her comments on the manuscript.

Supported by the National Framework Program for Research and Innovation PON (Grant 01_00110), the Italian Ministry of Health (5×1000 funding), Fondazione Roma, and the Irish Research Council (GOIPG/2013/775).

Disclosure: **D. Giannini**, None; **G. Lombardo**, None; **L. Mariotti**, None; **N. Devaney**, None; **S. Serrao**, None; **M. Lombardo**, None

References

1. Carroll J, Kay D, Scoles D, Dubra A, Lombardo M. Adaptive optics retinal imaging. Clinical opportunities and challenges. *Curr Eye Research*. 2013;38:709–721.
2. Lombardo M, Serrao S, Devaney N, Parravano M, Lombardo G. Adaptive optics technology for high-resolution retinal imaging. *Sensors*. 2013;13:334–366.
3. Roorda A, Duncan JL. Adaptive optics ophthalmoscopy. *Annu Rev Vis Sci*. 2015;1:19–50.
4. Duncan JL, Zhang Y, Gandhi J, et al. High-resolution imaging with adaptive optics in patients with inherited retinal degeneration. *Invest Ophthalmol Vis Sci*. 2007;48:3283–3291.
5. Garrioch R, Langlo C, Dubis AM, Cooper RF, Dubra A, Carroll J. Repeatability on in vivo cone density and spacing measurements. *Optom Vis Sci*. 2012;89:632–643.
6. Lombardo M, Lombardo G, Schiano Lomoriello D, Ducoli P, Stirpe M, Serrao S. Interocular symmetry of parafoveal photoreceptor cone density distribution. *Retina*. 2013;33:1640–1649.
7. Talcott KE, Ratnam K, Sundquist SM, et al. Longitudinal study of cone photoreceptors during retinal degeneration and in response to ciliary neurotrophic factor treatment. *Invest Ophthalmol Vis Sci*. 2011;52:2219–2226.
8. Zhang T, Godara P, Blanco ER, et al. Variability in human cone topography assessed by adaptive optics scanning laser ophthalmoscopy. *Am J Ophthalmol*. 2015;160:290–300.
9. Lombardo M, Serrao S, Ducoli P, Lombardo G. Influence of sampling window size and orientation on parafoveal cone packing density. *Biomed Opt Express*. 2013;4:1318–1331.
10. Lombardo M, Serrao S, Lombardo G. Technical factors influencing cone packing density estimates in adaptive optics flood illuminated retinal images. *PLoS One*. 2014;9:e107402.
11. Chiu SJ, Lokhnygina Y, Dubis AM, et al. Automatic cone photoreceptor segmentation using graph theory and dynamic programming. *Biomed Opt Express*. 2013;4:924–937.
12. Mariotti L, Devaney N, Lombardo G, Lombardo M. Understanding the changes of cone reflectance in adaptive optics flood illumination retinal images over 3 years. *Biomed Opt Expr*. 2016;7:2807–2822.
13. Cooper RF, Wilk MA, Tarima S, Carroll J. Evaluating descriptive metrics of the human cone mosaic. *Invest Ophthalmol Vis Sci*. 2016;57:2992–3001.
14. Zayit-Soudry S, Sippl-Swezey N, Porco TC, et al. Repeatability of cone spacing measures in eyes with inherited retinal degenerations. *Invest Ophthalmol Vis Sci*. 2015;56:6179–6189.
15. Chui TY, Song H, Burns SA. Individual variations in human cone photoreceptor packing density:variations with refractive error. *Invest Ophthalmol Vis Sci*. 2008;49:4679–4687.
16. Li KY, Tiruveedhula P, Roorda A. Intersubject variability of foveal cone photoreceptor density in relation to eye length. *Invest Ophthalmol Vis Sci*. 2010;51:6858–6867.
17. Hirsch J, Miller WH. Does cone positional disorder limit resolution? *J Opt Soc Am A*. 1987;4:1481–1489.
18. Rodieck RW. The density recovery profile: a method for the analysis of points in the plane applicable to retinal studies. *Vis Neurosci*. 1991;6:95–111.
19. Galli-Resta L, Novelli E, Kryger Z, Jacobs GH, Reese BE. Modelling the mosaic organization of rod and cone photoreceptors with a minimal-spacing rule. *Eur J Neurosci*. 1999;11:1461–1469.
20. Curcio CA, Sloan KR, Kalina RE, Hendrickson AE. Human photoreceptor topography. *J Comp Neurol*. 1990;292:497–523.
21. Ferris FL III, Wilkinson CP, Bird A, et al. Clinical classification of age-related macular degeneration. *Ophthalmology*. 2013;120:844–851.
22. Khan KN, Mahroo OA, Khan RS, et al. Differentiating drusen: drusen and drusen-like appearances associated with ageing, age-related macular degeneration, inherited eye disease and other pathological processes. *Prog Retin Eye Res*. 2016;53:70–106.
23. Early Treatment Diabetic Retinopathy Study Research Group. Grading diabetic retinopathy from stereoscopic color fundus photographs: an extension of the modified Airlie House classification. ETDRS report number 10. *Ophthalmology*. 1991;98(suppl):823–833.
24. Lombardo M, Parravano M, Serrao S, Ziccardi L, Giannini D, Lombardo G. Investigation of adaptive optics imaging biomarkers for detecting pathological changes of the cone mosaic in patients with type 1 diabetes mellitus. *PLoS One*. 2016;11:e0151380.
25. Ziccardi L, Giannini D, Lombardo G, et al. Multimodal approach to monitoring and investigating cone structure and function in an inherited macular dystrophy. *Am J Ophthalmol*. 2015;160:301–312.
26. Drasdo N, Fowler CW. Non-linear projection of the retinal image in a wide-angle schematic eye. *Br J Ophthalmol*. 1974;58:709–714.
27. Coletta NJ, Watson T. Effect of myopia on visual acuity measured with laser interference fringes. *Vision Res*. 2006;46:636–651.
28. Li KY, Roorda A. Automated identification of cone photoreceptors in adaptive optics retinal images. *J Opt Soc Am A*. 2007;24:1358–1363.

29. Lombardo M, Serrao S, Ducoli P, Lombardo G. Eccentricity dependent changes of density, spacing and packing arrangement of parafoveal cones. *Ophthalmic Physiol Optics*. 2013; 33:516–526.
30. Brostow W, Dussault JP, Fox BL. Construction of Voronoi polyhedra. *J Comput Physics*. 1978;29:81–92.
31. Lammer J, Prager SG, Cheney MC, et al. Cone photoreceptor irregularity on adaptive optics scanning laser ophthalmoscopy correlates with severity of diabetic retinopathy and macular edema. *Invest Ophthalmol Vis Sci*. 2016;57:6624–6632.
32. Yellott JI Jr. Spectral analysis of spatial sampling by photoreceptors: topological disorder prevents aliasing. *Vision Res*. 1982;22:1205–1210.
33. Lombardo M, Serrao S, Ducoli P, Lombardo G. Variations in the image optical quality of the eye and the sampling limit of resolution of the cone mosaic with axial length in young adults. *J Cataract Refract Surg*. 2012;38:1147–1155.
34. Muthiah MN, Gias C, Chen FK, et al. Cone photoreceptor definition on adaptive optics retinal imaging. *Br J Ophthalmol*. 2014;98:1073–1079.
35. Cooper RF, Lombardo M, Carroll J, Sloan KR, Lombardo G. Methods for investigating the local spatial anisotropy and the preferred orientation of cones in adaptive optics retinal images. *Vis Neurosci*. 2016;33:E005.
36. Curcio CA, Sloan KR. Packing geometry of human cone photoreceptors: variation with eccentricity and evidence of local anisotropy. *Vis Neurosci*. 1992;9:169–180.
37. Shapiro MB, Schein SJ, De Monasterio FM. Regularity and structure of the spatial pattern of blue cones of macaque retina. *J Am Stat Assoc*. 1985;80:803–812.
38. Duyckaerts C, Godefroy G. Voronoi tessellation to study the numerical density and the spatial distribution of neurones. *J Chem Neuroanat*. 2000;20:83–92.
39. Cook JE. Spatial properties of retinal mosaics: an empirical evaluation of some existing measures. *Vis Neurosci*. 1996;13: 15–30.
40. Putnam NM, Hofer HJ, Doble N, Chen L, Carroll J, Williams DR. The locus of fixation and the foveal cone mosaic. *J Vis*. 2005;5:632–639.
41. Scoles D, Sulai YN, Langlo CS, et al. In vivo imaging of human cone photoreceptor inner segments. In vivo imaging of photoreceptor inner segments. *Invest Ophthalmol Vis Sci*. 2014;55:4244–4251.

Investigative Ophthalmology & Visual Science